Chaotic flow and efficient mixing in a microchannel with a polymer solution

Teodor Burghelea,[1] Enrico Segre,[2] Israel Bar-Joseph,[3] Alex Groisman,[4] and Victor Steinberg[1]
[1]*Department of Physics of Complex Systems, Weizmann Institute of Science, Rehovot, 76100 Israel*
[2]*Department of Physical Services, Weizmann Institute of Science, Rehovot, 76100 Israel*
[3]*Department of Condensed Matter Physics, Weizmann Institute of Science, Rehovot, 76100 Israel*
[4]*Department of Physics, UCSD, 9500 Gilman Dr., La Jolla, California 92093-0374, USA*
(Received 18 December 2003; published 11 June 2004)

Microscopic flows are almost universally linear, laminar, and stationary because the Reynolds number, Re, is usually very small. That impedes mixing in microfluidic devices, which sometimes limits their performance. Here, we show that truly chaotic flow can be generated in a smooth microchannel of a uniform width at arbitrarily low Re, if a small amount of flexible polymers is added to the working liquid. The chaotic flow regime is characterized by randomly fluctuating three-dimensional velocity field and significant growth of the flow resistance. Although the size of the polymer molecules extended in the flow may become comparable to the microchannel width, the flow behavior is fully compatible with that in a macroscopic channel in the regime of elastic turbulence. The chaotic flow leads to quite efficient mixing, which is almost diffusion independent. For macromolecules, mixing time in this microscopic flow can be three to four orders of magnitude shorter than due to molecular diffusion.

DOI: 10.1103/PhysRevE.69.066305 PACS number(s): 47.27.−i, 47.50.+d, 83.50.−v

I. INTRODUCTION

Flows of liquids in microscopic channels have been attracting increasing interest recently due to fast development of microfluidics and soft lithography [1,2]. The microfluidic devices, which are becoming increasingly advanced and reliable, allow dramatic reduction of amounts of reagents required for fine chemistry and biochemistry [3], well-controlled manipulation and sophisticated experiments on individual cells [4–6] and macromolecules [7]. The microscopic flows are almost universally laminar, with linear dependence of the flow rate on the driving force. They also usually remain steady as long as the driving force does not change. All of that has to do with low to moderate values of the Reynolds number, $\mathrm{Re}=Vd\rho/\eta$, which is a general measure of nonlinear inertial effects in the flow and of the likelihood to find it being chaotic or turbulent [8]. Here, V is the flow velocity, d is the diameter of the channel, and ρ and η are the density and the viscosity of the fluid, respectively. When d is reduced, the flow velocity needed to reach a given high Re, which is required to generate chaotic or turbulent flow, increases as d^{-1}. The driving pressure per unit length scales as $\Delta P/\Delta L \sim \eta V/d^2$, giving $\Delta P \sim \Delta L/d^3$ at a given Re in the channel. Therefore, if the channel proportions are preserved, ΔP grows quadratically with d^{-1}, and when the channels are only a few tens of microns wide, achieving sufficiently high Re requires impractically high driving pressures.

The laminar character of microscopic flows has multiple practical advantages including possibility of precise control of flow velocity, chemical concentration profiles [4–6], and targeted delivery of chemicals and particles [5]. On the other hand, the laminar flows have an inherent problem of inefficient mass transfer in directions perpendicular to the main flow, which occurs due to molecular diffusion only. Diffusion time, d^2/D, across a typical microchannel with a width of 100 μm is on the order of 100 s even for moderate size proteins, such as bovine serum albumin with a diffusion coefficient of $D \approx 3\times 10^{-7}$ cm^2/s in water [9].

A few techniques have been proposed to generate stirring by a three-dimensional flow in order to increase the rate of mixing in the microchannels. They include application of time-dependent external forces [10,11] and raising Re to moderately high values in curvilinear three-dimensional channels [12,13]. An ingenious method of mixing has been suggested recently, which involves special "herringbone" patterning of a microchannel wall to generate fluid motion perpendicular to the main flow direction in the linear, low Re regime [14]. The fluid elements are continuously stretched and folded in the flow as they advance along the channel. That separates closely spaced fluid particles and brings distant particles together, dramatically reducing the characteristic length scales and diffusion time and increasing the rate of homogenization of the mixture. The flow was stationary in the laboratory frame, however. Therefore, the concentration profiles of the fluorescent dye used as a tracer were uniquely defined by the entrance conditions and the channel geometry [14]. They did not change in time, and there was always some constant difference in concentration between neighboring points.

The basic condition of linearity in low Re flows can be changed by adding flexible, high molecular weight polymers to the working liquid [15]. Solutions of those polymers are known as non-Newtonian visco-elastic fluids [15]. Mechanical stress in these fluids depends on the flow history with some characteristic relaxation time, λ, which for dilute solutions is a time of relaxation of individual polymer molecules. Another specific property of the polymer solutions is the nonlinear dependence of the polymer contribution to the stress on the rate of deformation in the flow, ∇V [15]. This nonlinearity usually becomes significant when the Weissenberg number, $\mathrm{Wi}=\lambda\nabla V$, becomes on the order of unity. The nonlinear growth of the elastic polymer stresses is especially striking in extensional flows at $\mathrm{Wi}>1/2$, where apparent viscosity of polymer solutions can rise by up to three orders of magnitude as the total deformation increases [16]. In pure

shear flows the major nonlinear elastic effect shows up in the appearance of negative normal stress along the flow direction. It leads to the well-known effect of rod climbing [15,17] and causes purely elastic instabilities in curvilinear flows of viscous polymer solutions in macroscopic setups, when inertial effects are virtually absent [18]. The non-linear polymer stresses in curvilinear shear flows can also lead to elastic turbulence, a random multiscale three-dimensional flow, which can develop at arbitrarily low Re [19]. Elastic turbulence causes sharp growth of the flow resistance [19,20], and it was found to generate efficient mixing in a macroscopic curvilinear channel [21].

Recently, it was shown that the nonlinear elasticity of the polymer solutions can cause a purely elastic transition and nonlinear growth of flow resistance in a microscopic channel with contractions [22]. Those nonlinear effects, however, were due to regions of fast extensional flow near the contractions, where individual polymer molecules are expected to partially unravel at $\mathrm{Wi} > 1/2$ [23,24]. The nonlinearity in resistance was the most dramatic feature of the transition, and it became quite significant before any substantial changes in the flow pattern could be seen [22]. Therefore, the nonlinear resistance could be understood as a simple additive effect of individual molecules forced through the contractions. Although the flow became rather irregular at higher flow rates, the fluctuating flow regions were mostly near the contractions, and no detailed study of those fluctuations was made.

If the basic linear flow is a pure shear as in Refs. [19–21], a nonlinear elastic transition can only occur through a major reorganization of the flow structure. In Refs. [19–21] the secondary flow generated above the instability threshold had well-expressed turbulent features and involved irregular fluid motion in a broad range of temporal and spatial scales. That implies an essentially collective effect of the polymer molecules on the flow, and the polymer solution behaving as a visco-elastic continuum. If the size of the setup is reduced to a microscale, nonhomogeneity in the polymer concentration and extension of polymer molecules stretched in the flow may become comparable with the size of the setup, and larger than the size of some of the generated vortices. Therefore, whether or not the purely elastic instability and elastic turbulence can be reproduced in a microscopic shear flow is still an open question.

Here, we show that a fully developed chaotic flow similar to the elastic turbulence can be generated in a flat, curvilinear microscopic channel with smooth walls and uniform width at arbitrarily low Re, if the working liquid contains a small amount of high molecular weight polymers. The flow is characterized by significant nonlinear growth in resistance, randomly fluctuating velocity field, and chaotic three-dimensional mixing patterns. It is further shown that stirring by the flow results in efficient mixing in the microchannel with characteristic mixing length significantly shorter compared with the herringbone patterning method reported before [14]. The characteristic mixing times for solutions of macromolecules are reduced by three to four orders of magnitude compared with molecular diffusion.

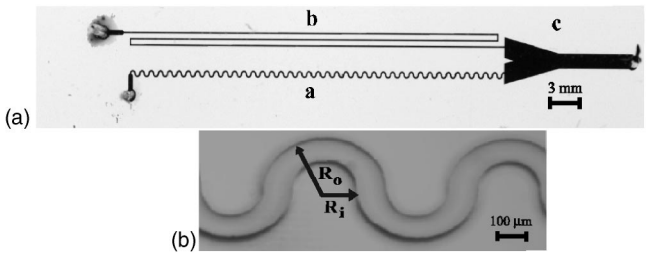

FIG. 1. (A) Photograph of the microfluidic device. The microchannels were filled with ink for better contrast. (B) Magnified image of a section of the functional curvilinear channel. The point where instantaneous flow velocity measurements, averaged over a 20×20 μm square region, were made is marked by a small cross.

II. MATERIALS AND METHODS

A. Device fabrication

The microchannel devices consist of a silicon elastomer (Sylgard 184 by Dow Corning) chip sealed to a #1 microscope cover glass. The channel structure of the chip was fabricated using the technique of soft lithography [1]. First, a negative master mold was fabricated in UV-curable epoxy (SOTEC micro-systems SU8-1070) by using conventional photolithography. The epoxy was spun onto a silicon wafer at 1800 rpm for 60 s to create a 100-μm layer and patterned by using a high-resolution negative transparency mask. Liquid elastomer was poured on the mold to a thickness of ≈5 mm and cured in an 80 °C oven for l h 30 min. After that the elastomer was peeled off the mold, trimmed to its final size, and liquid feeding ports were punched by using a 20-gauge Luer stub. The patterned side of the chip was bonded to the cover glass by overnight baking in the 80 °C oven.

B. Experimental setup

A snapshot of our first microfluidic setup is shown in Fig. 1. It has a uniform thickness $d = 100$ μm. Its main active element is a curvilinear channel with square cross section. It is a chain of 40 identical segments, which are couples of interconnected half-rings with inner and outer radii $R_i = 100$ μm and $R_o = 200$ μm, respectively [Fig. 1(B)]. It has the same proportions as the macroscopic channel, which was used in the elasticity induced mixing experiments reported before [21], but its dimensions are reduced by a factor of 30. Because of the periodic structure of the channel, it is convenient to use the number of a segment, N, starting from the inlet as a discrete linear coordinate along the channel. The auxiliary rectilinear channel (b) has width of 90 μm and total length of about 72.5 mm. Channel (b) and the comparator region (c) serve to make differential *in situ* measurements of flux vs pressure by the method described in Ref. [22].

C. Flow control

The flow in the microchannels was generated and controlled by pressure differences between the inlets and the outlet [Fig. 1(A)]. The pressures were generated hydrostatically using long vertical rails with precise rulers and sliding stages. Working liquids were kept in 30-ml plastic syringes,

which were held upright, open to the atmosphere, and connected to the two inlets and the outlet by plastic tubing with internal diameter of 0.76 mm. The pressure drop in the tubing was estimated below 1% of the total. The two syringes feeding the inlets were attached to the sliding stages. The difference in liquid elevation between these two syringes and the outlet syringe was measured and adjusted with a precision of about 0.1 mm, corresponding to 1 Pa in pressure. Dependence of the volumetric low rate, Q, in the curvilinear channel on the pressure difference between inlet 1 and outlet, Fig. 1, was determined with a relative precision of about 0.5% using an *in situ* measurement technique described elsewhere [22]. A syringe pump (PHD 2000 by Harvard Apparatus Inc.) with a 50-ml gas-tight Hamilton syringe was used for an absolute flow rate calibration.

D. Polymer solutions

The polymer used was polyacrylamide, PAAm, by Polysciences Inc. with high molecular weight $M_w = 1.8 \times 10^7$, which was the same polymer sample as in Ref. [21]. It was dissolved at identical concentrations of 80 ppm by weight in two Newtonian solvents with different viscosities. The solvent for the low viscosity solution 1 was a 35% solution of sucrose in water with 1% of NaCl added to fix the ionic contents. The Newtonian viscosity of the solvent, η_s, was 4.2 mPa at the room temperature of 22 °C. The viscosity of solution 1, η, was 5.6 mPa at a shear rate of 50 s^{-1}, suggesting a dilute polymer solution. The Newtonian solvent for the high viscosity solution 2 was sugar syrup containing 64.4% sucrose and 1% of NaCl in water. The viscosity of solvent 2 was 114 mPa at 22 °C, and the viscosity of solution 2 was 138 mPa at a shear rate of 2 s^{-1}. The polymer relaxation time, λ, of solution 2 measured by phase shift between stress and shear rate in an oscillatory flow regime was 1.1 s. The measurements of viscosity and relaxation time were made using a high-precision rheometer (AR1000 by TA Instruments). Relaxation time of solution 1 was estimated as 0.04 s with the assumption that λ scales linearly with η_s [15].

The overlap concentration c^*, taken as a concentration at which the viscosity ratio reached $\eta/\eta_s = 2$, was 200 ppm by weight for solvent 2, corresponding to molecular concentration of $n = 8.76 \times 10^{12}$ cm^{-3}. Characteristic size of the polymer coils at rest can be estimated from this as $n^{-1/3} \approx 0.5$ μm, and characteristic distance between them at 80 ppm by weight can be estimated as 0.7 μm. These estimates are well supported by the data on PAAm taken from the literature [25]. One can use the Mark-Houwink scaling relation for PAAm, $[\eta] = 6.31 \times 10^{-3} M_w^{0.8}$ (in ml/g) [25], where $[\eta]$ is the intrinsic viscosity of the polymer defined as $[\eta] = (\eta - \eta_s)/c\eta_s|_{c \to 0}$. At molecular weight $M_w = 1.8 \times 10^7$ one gets $[\eta] = 4020$ ml/g. Defining $c^* = 1/[\eta]$ [15] we obtain $c^* = 250$ ppm by weight for an aqueous solution, in good agreement with the above estimate. Further, we can compare the estimated size of the PAAm coils with the data obtained from light scattering, Ref. [25]. Plugging $M_w = 1.8 \times 10^7$ into an interpolation relation from Ref. [15], one gets $R_g \approx 0.4$ μm for the radius of gyration of the coils, which is rather consistent with the above estimate obtained from c^*.

It is worth noting that $c^* = 200$ ppm is very close to the value found for λ-phage DNA [26], which has a comparable molecular weight of 3.1×10^7. Radius of gyration of the λ-phage DNA was found to be 0.73 μm [27], which is quite in line with the above estimate for the PAAm coil size. The full contour length of a PAAm molecule having $M_w = 1.8 \times 10^7$ and thus consisting of 2.5×10^5 monomers (having molecular weight 71.08 g/mol) can be estimated as about 50 μm, if a monomer length of 0.2 nm is assumed. It is significantly larger than the contour length of the λ-phage DNA (which is equal to about 16 μm) and twice as small as the microchannel diameter.

The experiments on mixing were carried out with polymer solution 2, and then fluorescent dyes with low diffusivities were added to the solution and used as tracers. Those were a few different samples of fluorescein-conjugated Dextran, FITCD, by Sigma with average molecular weights, M, varying from 10 kDa to 2 MDa. In spite of the relatively high molecular weight of FITCD, it did not have any measurable influence on the solution rheology due to high rigidity of the polysaccharide molecules. Diffusion coefficients of the FITCD samples in water were estimated using the data in Ref. [28], giving values from 9.1×10^{-7} to 7.4×10^{-8} cm^2/s that corresponded to a broad range of biological macromolecules. The diffusion coefficients in solvent 2 were estimated with the assumption that $D \sim 1/\eta_s$, resulting in $D_1 = 6.6 \times 10^{-9}$ and $D_2 = 5.4 \times 10^{-10}$ cm^2/s for 10 kDa and 2 MDa FITCD, respectively.

E. Measuring flow velocity

Measurements of the flow velocity in the microchannel were carried out using custom-developed microscopic particle image velocimetry, micro-PIV. The polymer solution was seeded with 0.2 μm yellow-green fluorescent beads (Polysciences), and epi-fluorescent imaging of the flow in the microchannel, Fig. 1, was made with an inverted microscope (Olympus IMT2) and narrow-band excitation and emission filters in the dichroic filter cube. The objective was a LWD 20×, NA = 0.40, and the images were projected onto a CCD array with 640 × 480 pixel resolution (PixelFly camera by PCO, Germany) and digitized to 12 bits. The snapshots of the flow were taken with even time intervals of 40 ms, and digitally postprocessed. Images of out-of-focus particles were disregarded. Velocity field was found by cross correlating positions of the particles in two consecutive snapshots, and the particle velocity vectors were neighbor validated. (The calculated velocity field corresponded to the time interval between the two snapshots.) The collected time series represent velocity averaged over a 20×20 μm square region at the middle plane of the channel. Its position in the channel is shown by a little cross in Fig. 1(B): it is equidistant with respect to the channel walls(at $R = 150$ μm) and at equal distances from interconnections of two half-rings at $N = 35$.

F. Measuring tracer concentration profiles

Concentrations of the fluorescent dyes, which were used as passive tracers in the experiments on mixing in the channel, were measured using a commercial confocal microscope

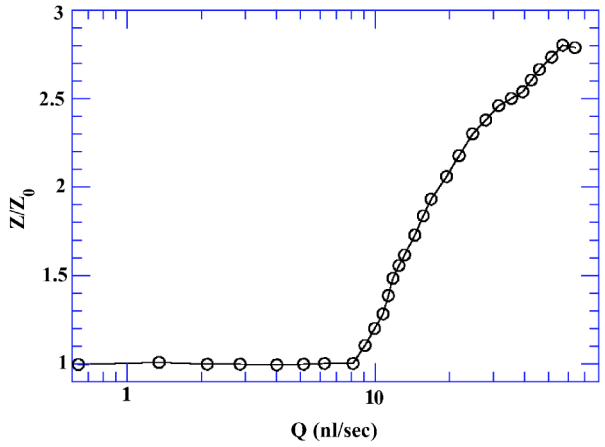

FIG. 2. Dependence of normalized resistance, Z/Z_0, in flow of solution 1 through the curvilinear channel on the volumetric flow rate, Q, in semilogarithmic scale.

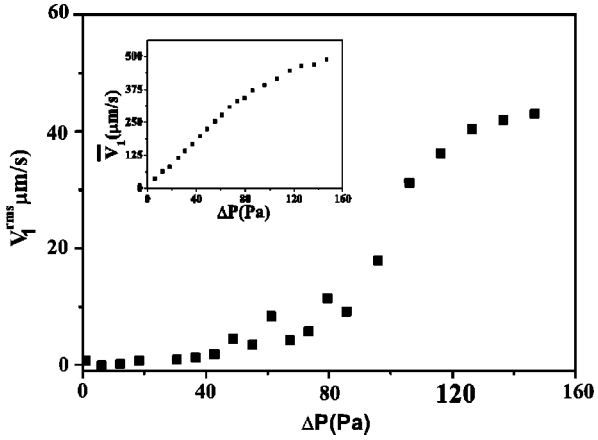

FIG. 3. Dependence of rms of fluctuations of the longitudinal component of flow velocity, V_1^{rms}, on pressure drop per segment, ΔP, in the center of the microchannel for solution 2. Inset: Dependence of time average of the the longitudinal flow velocity, $\overline{V_1}$, in the center of the microchannel on ΔP.

(Fluoview FV500 by Olympus). It was equipped with a 40 $\times$NA=0.85 infinity corrected objective and a 12-bit photomultiplier. The scanning was done at a rate of 56 lines per second and 512 pixels per line corresponding to a step of 0.18 μm per pixel.

III. RESULTS

We measured volumetric flux rate, Q, of solution 1 through the curvilinear channel, Fig. 1, in a broad range of applied pressures and calculated the resistance factor, $Z=\Delta P/Q$, where ΔP is pressure drop per segment. The resistance factor is a constant proportional to viscosity for Newtonian fluids in linear, low Re regime, and it can be used as a measure of turbulent flow resistance in large channels at high Re. Figure 2 shows dependence of Z on Q for solution 1, after Z is divided by a resistance factor, Z_0, found for a Newtonian liquid with the same viscosity, η. The ratio Z/Z_0 is constant equal to unity in the linear regime at low Q. At Q of about 8.5 nl/s, however, a nonlinear transition occurs; Z/Z_0 starts to grow and reaches a factor of about 2.8 at high Q. The Reynolds number for the channel flow can be defined as $\mathrm{Re}=Q\rho/(\eta d)$. It was 0.017 at the transition point and 0.14 at the highest Q that we tried, so that the inertial effects were always negligible. The Weissenberg number can be defined as $\mathrm{Wi}=4\lambda Q/d^3$, and its estimated value at the transition point is 1.4, which is comparable with Wi found at purely elastic transitions in macroscopic setups [18,19,21,29].

In order to get detailed information about structure of the flow above the nonlinear transition, we used solution 2 with high viscosity and large λ. The polymer relaxation time, λ, defines a characteristic velocity d/λ, which sets a scale for the average flow velocity at transition to the elastic nonlinear regime [15,29]. Further, λ sets a scale of time for fluctuations (or oscillations) in the flow above the elastic transition [29]. Therefore, characteristic velocities in the nonlinear flow in solution 2 were expected to be much lower, and measurements of different fluctuating parameters were expected to be more feasible with the standard video microscopy techniques. Using the micro-PIV we measured flow velocity in the middle of the curvilinear channel, where velocity is maximal. Dependence of rms of fluctuations of the longitudinal component of the flow velocity, V_1^{rms} (which is the velocity component along the main flow) on ΔP is shown in Fig. 3. The fluctuations are virtually absent in the linear regime at low pressure. At ΔP of about 50 Pa, however, V_1 starts to fluctuate, and V_1^{rms} begins to grow quickly and nonlinearly. It can be learned from the inset in Fig. 3 that the time-averaged longitudinal velocity, $\overline{V_1}$, grows linearly at low ΔP, but its growth slows down at the same critical ΔP of about 50 Pa, which is further evidence for a nonlinear elastic flow transition taking place. We used micro-PIV to measure average longitudinal flow velocity in different points across the channel at the flow transition. A cross-channel space-time average obtained with the longitudinal velocity method was about 80 μm/s. That gives estimates of $Q\approx 0.8$ nl/s, $\mathrm{Re}\approx 8\times 10^{-5}$, and $\mathrm{Wi}\approx 3.5$ for the elastic nonlinear transition. This value of the Weissenberg number is very close to $\mathrm{Wi}_c\approx 3.2$ found for the transition to chaotic flow in the macroscopic curvilinear channel in Ref. [21].

A typical time series of the instantaneous velocity V_1 above the transition is shown in Fig. 4(A). The velocity is strongly fluctuating and its time dependence has well-expressed chaotic appearance. The chaotic character of the velocity fluctuations is confirmed by analysis of its time correlations. The velocity autocorrelation function shown in Fig. 4(B) does not have distinct peaks and decays uniformly.

For the experiments on mixing, the design of the microchannel was slightly modified to enable side-by-side injection of two streams of solution 2, one with and one without FITCD, to the channel inlet, Fig. 5(A). Apart from $c_0=280$ ppm by weight of FITCD added to one of them, the polymer solutions were identical and were injected at equal flow rates by careful adjustment of the driving pressures, Fig. 5(A). The setup was first tested with the plain solvents without PAAm added. The flow appeared laminar at all ΔP that we applied, and the interface between the streams with and without FITCD remained smooth and sharp along the whole

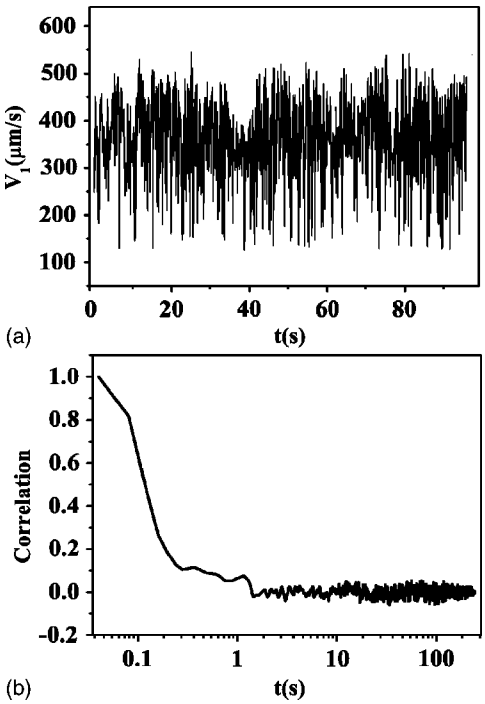

FIG. 4. (A) Time series of the longitudinal flow velocity, V_1, in the center of the microchannel at $\Delta P = 100$ Pa. (B) Autocorrelation function for V_1 based on about 6000 individual velocity measurements.

channel with only minor smearing by diffusion, Fig. 5(B).

The situation was similar with the polymer solutions in the linear regime at low ΔP. However, when the driving pressure was raised above the nonlinear transition threshold, fluctuating flow velocity produced significant stirring and complex and chaotically changing tracer concentration pro-

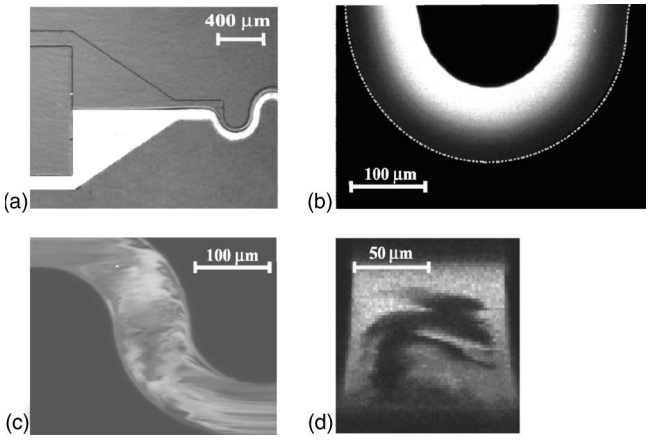

FIG. 5. (A) Epifluorescent microphotograph of the entrance area of a microchannel used in experiments on mixing. Wide triangular region in front of a curvilinear channel allows to adjust equal flow rates for polymer solutions with (from below) and without FITCD. (B) Confocal photograph of flow in the microchannel without polymers added. Right wall of the channel is shown by a dotted line from below. (C) Confocal image of mixing in chaotic flow in the microchannel with solution 2 in it. (D) Confocal image of crosssection of the microchannel with chaotic flow in solution 2.

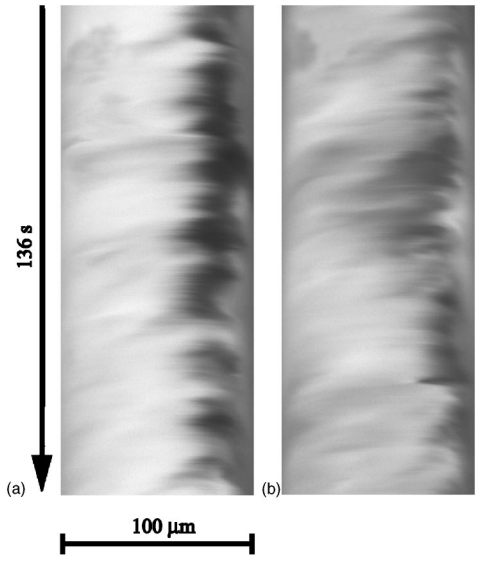

FIG. 6. Space-time plots of FITCD distribution across the channel taken at (A) $N = 12$ and (B) $N = 18$. Confocal scanning was done along the same line across the channel in the midplane at equal distances from half-ring interconnections, with even time intervals of 0.0177 s. Profiles of FITCD concentration in consecutive moments of time are plotted from top to bottom.

files, Figs. 5(C) and 5(D). Here, mixing of FITCD of 2 MDa molecular weight at $\Delta P = 248$ Pa is studied.

The confocal scans in a horizontal plane, Fig. 5(C), was made at a scanning rate of 56 lines per s, contained 750 individual lines, and took about 13 s to complete. The vertical scan, Fig. 5(D), was performed with a scanning rate of 24 lines pers, contained 45 lines, and took about 1.8 s to complete. Characteristic time of concentration variation was estimated as about 2.5 s (Fig. 6). Therefore, although individual vertical lines in Fig. 5(C) and horizontal lines in Fig. 5(D) represent virtually instantaneous dye distributions, the 2D concentration diagrams in Figs. 5(C) and 5(D) should not be considered as snapshots and are shown for the purpose of illustration only.

We studied in detail mixing of FITCD with 2 MDa molecular weight in the channel at $\Delta P = 124$ Pa, corresponding to a flow rate about twice above the nonlinear transition threshold (cf. Ref. [21]) and the cross-channel space-time averaged longitudinal velocity of about 173 μm/s. Variation of the tracer concentration profiles with time at different distances from the inlet is illustrated by the space-time plots in Figs. 6(A) and 6(B). One can observe that the tracer concentration appears to fluctuate quite randomly without any apparent scale in time or space. Next, one can see in Fig. 6(A), taken at $N = 12$, that the left side of the channel, where the tracer was initially injected, looks much brighter and has much higher average concentration of the tracer. Although also noticeable in Fig. 6(B) taken further downstream, at $N = 18$, this feature is clearly weaker there. Thus, stirring by the fluctuating velocity field seems to create a more symmetric distribution of the tracer between the two sides of the channel. In order to validate this observation, we measured time averages of the tracer concentration, $\overline{c}$, at different positions across the channel and at different N, Fig. 7(A). One can see

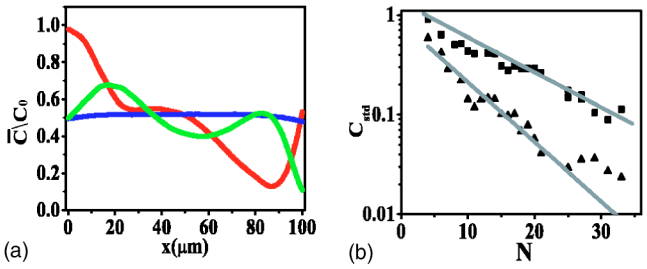

FIG. 7. (A) Time average of FITCD concentration, $\overline{c}$, divided by c_0, as a function of position, x, along a line across the channel taken at different distances from the inlet: $N=7$, $N=11$, and $N=41$. The lines across the channel were in the midplane at equal distances from half-ring interconnections, just as for the space-time plots in Fig. 6. (B) Standard deviation of FITCD concentration from its average value, c_{std}, as a function of distance, N, from the inlet for two kinds of FITCD with average molecular weights of 10 kDa (triangles) and 2 MDa (squares).

that the cross-channel distribution of $\overline{c}/c_0$ close to the inlet, at $N=7$, is strongly influenced by the asymmetric conditions at the channel entrance. As one can learn from the curve at $N=11$, however, the imprint of the initial conditions is clearly fading as the liquid advances downstream and is stirred. Further downstream, at $N=41$, asymmetry in the tracer distribution introduced by the initial conditions disappears completely. Fading of the initial condition influence with time and restoration of symmetry in flow in the statistical sense are both distinct features of chaotic and turbulent flows. Therefore, the curves in Fig. 7(A) provide further evidence for truly chaotic nature of the flow in the microchannel.

A natural parameter characterizing inhomogeneity of the mixture is standard deviation of the instantaneous local tracer concentration, c, from its overall average value $\langle c\rangle = c_0$. It is convenient to divide it by $\langle c\rangle$ and to introduce a dimensionless standard deviation $c_{\mathrm{std}}=\sqrt{\langle (c-\langle c\rangle)^2\rangle}/\langle c\rangle$. At the channel entrance c_{std} is equal to unity, and it becomes zero when the liquid is perfectly mixed and homogeneous. Dependence of c_{std} on N for two tracers with diffusion coefficients of $D_1=6.6\times10^{-9}$ and $D_2=5.4\times10^{-10}$ cm^2/s is shown in Fig. 7(B) in semilogarithmic scale. Each point in Fig. 7(B) is based on statistics over 10 000 individual cross-channel profiles (of the type shown in Fig. 6) taken in consecutive moments of time at a rate of 56 lines per s. In order to avoid possible artifacts due to image aberrations near the channel side walls, the regions near the walls with widths of $0.1d$ were excluded from the statistics. The total averaging time was 177 s, corresponding to about 70 characteristic concentration fluctuation times and an integral fluid discharge of about $300d^3$ (cf. Ref. [21], Fig. 3). Confocal scans of the channel cross sections similar to that in Fig. 5(D) were made at a few positions, N, from 5 to 35. Homogeneity of the dye concentration over the cross sections was always similar to that in the space-time plots taken in the midplane of the channel (Fig. 6) at the same N. In particular, no special unmixed spots with persistently high fluctuations of c (or deviations of c from the average) were found in the channel cross sections, other than in regions near the channel walls [30]. No extensive statistics on the dye distributions over the channel cross sections were collected, though.

One can see that the mixture becomes increasingly homogeneous as the liquid advances downstream, and the parameter c_{std} decays exponentially with N for both tracers. An exponential decay was also found in the case of elastic turbulence in a macrochannel [21], and it agrees very well with theoretical predictions for the so-called Batchelor regime [31–34] of mixing. The latter corresponds to a flow, which is chaotic in time but essentially "smooth" in space, in the sense that small eddies are rare, and the main contribution to mixing comes from the largest eddies having the size of the whole system.

The rates of the exponential decay for the two dependencies shown in Fig. 7(B) were 0.217 and 0.137, corresponding to ΔN of 4.61 and 7.30, and lengths $L_1=4.34$ and $L_2=6.88$ mm, respectively. The latter can be considered as characteristic mixing distances along the channel for the two tracers. Characteristic mixing times, which can be estimated as $t_{\mathrm{mix}}=L/\overline{V}$, are then found to be $t_{\mathrm{mix},1}=25$ s and $t_{\mathrm{mix},2}=40$ s, respectively. In the absence of active stirring, mixing would only occur through molecular diffusion, with characteristic diffusion times across the channel given by $t_{\mathrm{diff}}=d^2/D$ resulting in $t_{\mathrm{diff},1}=1.5\times10^4$ s and $t_{\mathrm{diff},2}=1.9\times10^5$ s, respectively. Therefore, the stirring produced by the chaotic flow in the channel reduces the mixing times for the FITCD macromolecules by three to four orders of magnitude.

IV. DISCUSSION

We studied flow of two dilute polymer solutions in a microscopic curvilinear channel. We observed a nonlinear transition to occur in the flow at $\mathrm{Re}\approx1.7\times10^{-2}$, $\mathrm{Wi}\approx1.4$, and $\mathrm{Re}\approx8\times10^{-5}$, $\mathrm{Wi}\approx3.5$, for solution 1 and solution 2, respectively. The very small and different values of Re, and comparable order of unity values of Wi at the transition threshold for the two solutions indicate that the transition is of purely elastic nature and can occur at arbitrarily low Re. A possible explanation of the difference in estimated critical Wi for the two polymer solutions is that the actual polymer relaxation time of solution 1 may be significantly higher than the estimate based on the assumption that $\lambda\sim\eta_s$.

A major global feature of the flow above the nonlinear elastic transition is fast growth of the resistance, Fig. 2. It increases by up to a factor of 2.8 above the resistance for a Newtonian fluid with the same shear flow viscosity, η, at the same Q. Since Re is very low, the whole growth of the flow resistance should be due to increase in the elastic polymer stresses [20]. In a pure shear flow with $\dot{\gamma}=240$ s^{-1}, corresponding to $Q=60$ nl/s (and $\mathrm{Wi}\approx10$), viscosity ratio for polymer solution 1 was $\eta/\eta_s=1.22$. Hence, the average increase in the polymer shear stresses due to the secondary flow at $Q=60$ nl/s (Fig. 2) can be estimated as a factor of about 11. Suggesting linear deformation of the flexible polymer molecules in a shear flow at low to moderate Wi [35], we can estimate extension of the molecules at $\mathrm{Wi}=10$ as 10×0.5 μm$=5$ μm. (Flexible polymer molecules were found to extend linearly with the shear rate, until the extension reached 15%–20% of their full length [35].) Additional

extension of the polymers due to the irregular secondary flow, as suggested by the stress growth by the factor of 11, can be estimated as a factor of $\sqrt{11}$ (suggesting that the secondary flow results in an isotropic polymer unraveling and the stress grows as a square of the polymer extension [15]). That brings characteristic size of the extended polymer molecules to 20 μm range, less than an order of magnitude smaller than the diameter of the channel, $d=100$ μm.

The growth of the elastic stresses due to the fluctuating secondary flow can only occur as a result of significant reorganization of the flow structure and spontaneous generation of regions with strong extensional flow, as in the case of the elastic turbulence [19,20]. (In shear flows polymer contribution to resistance increases slower than linearly with the shear rate, which is called shear thinning.) This suggestion is quite corroborated by the direct flow velocity measurements in solution 2 above the nonlinear transition. Velocity is found to be strongly fluctuating, Figs. 3 and 4, with rms of the fluctuations reaching as much as 10% of the mean longitudinal velocity at the center of the channel, Fig. 3, just as in the macroscopic channel in Ref. [21]. The velocity appears to vary randomly in time, Fig. 4(A), and its autocorrelation function decays quite quickly and does not have any distinct peaks, Fig. 4(B). These all are clear indications of chaotic nature of the flow in the channel in the nonlinear regime at high Wi. Another evidence of chaos comes from the experiments on mixing, Figs. 6 and 7. Asymmetry in distribution of $\overline{c}/c_0$ across the channel, which is imposed by the conditions at the channel entrance, decays with the distance from the entrance, Fig. 7(A). Further, c_{std} exponentially decays with N, as it is supposed to be in the chaotic Batchelor regime of mixing [21,33,34].

Experimental results presented in Figs. 2–4 and Figs. 6 and 7 and discussed above are fully consistent with a suggestion that the regime of elastic turbulence [19] is being realized in the microchannel. In fact, the results in Figs. 2–4 and Figs. 6 and 7 agree rather well with the measurements in macroscopic systems reported before [19,20]. We find it rather remarkable that although the size of extended molecules may become comparable with the channel diameter, it does not seem to cause any significant new effects in the polymer solution dynamics. An essential feature of turbulent flows is a broad range of spatial scales, at which fluid motion is excited. Unfortunately, limited resolution of the micro-PIV technique did not allow us to explore properties of the flow down to sufficiently small spatial scales and to obtain conclusive data about its spatial structure. Therefore, we can only refer to the flow in the microchannel as being chaotic.

In the experiments with passive tracers, we found that stirring by the chaotic flow results in efficient mixing in the channel, Figs. 5–7. So, mixing times for the macromolecules, which we used as tracers, were reduced by three to four orders of magnitude compared with passive molecular diffusion, Fig. 7(B). It is worth noting that the characteristic distance of $\Delta N=7.3$ required for mixing of low diffusivity FITCD is comparable with $\Delta N\approx 15$ found in the chaotic flow in the macroscopic channel, Ref. [21]. We further notice that whereas the diffusion time scaled as $1/D$, the time of mixing in the chaotic flow depended on D very weakly. It increased by only 60% between the lower and upper curve in Fig. 7(B) (from $t_{\mathrm{mix},1}=25$ s and $t_{\mathrm{mix},2}=40$ s), whereas D dropped by a factor of 12 (from $D_1=6.6\times 10^{-9}$ to $D_2=5.4\times 10^{-10}$ cm^2/s). The weak dependence of t_{mix} on D is quite consistent with theoretical predictions for chaotic flows and the Batchelor regime [31–34]. It implies that the elasticity induced chaotic stirring in the microchannel can be efficiently used for mixing of liquids with additives of any low diffusivity, such as large molecules of DNA, viruses, particles, and possibly living cells.

The relatively long times of mixing in the chaotic flow of solution 2 are due to high viscosity of the solvent, large λ, and low flow velocity at the elastic instability threshold. In a much more practically relevant case of water-based solutions with the viscosity on the order of 0.001 P, λ is expected to be about 100 times lower and the flow velocities in the chaotic regime should be about 100 times higher [15,29]. Suggesting qualitatively similar flow conditions [29], we expect characteristic mixing times for the water-based solutions to be on a 100 ms scale. Since diffusion coefficients for macromolecules are proportional to $1/\eta_s$ [15], the ratio between t_{diff} and t_{mix} for the chaotic flow in the water-based solutions should be in the same range of 10^3 to 10^4.

The characteristic mixing length along the channel for water-based solutions should also remain in the same range of about 4–7 mm. It is about 2–3 times shorter than characteristic lengths in the herringbone patterned channel of Ref. [14] at comparable values of Peclet number, $\mathrm{Pe}=Vd/D$. Although the method of mixing by elasticity induced chaotic flow requires addition of polymers to the working liquid, it may be quite practical for many biochemical assays, taking into account the very low concentration of the high molecular weight polymers used. It does not rely on any special patterning of the microchannels and should be readily compatible with rounded channel profiles used for integrated microvalves and peristaltic pumps [36], allowing efficient mixing in closed-loop microscopic flows [37].

ACKNOWLEDGMENTS

We are grateful to M. Chertkov and V. Lebedev for many useful and illuminating discussions and to D. Mahalu for valuable help with the microfabrication. One of us (T. B.) thanks V. Kiss for his support in the confocal setup measurements. This work is partially supported by an Israel Science Foundation grant, Binational US-Israel Foundation, and by the Minerva Center for Nonlinear Physics of Complex Systems.

[1] Y. N. Xia and G. M. Whitesides, Annu. Rev. Mater. Sci. **28**, 153 (1998).
[2] G. M. Whitesides and A. D. Stroock, Phys. Today **54**(6), 42 (2001).
[3] C. L. Hansen, E. Skordalakes, J. M. Berger, and S. R. Quake, Proc. Natl. Acad. Sci. U.S.A. **99**, 16531 (2002).
[4] N. L. Jeon, H. Baskaran, S. K. W. Dertinger, G. M. Whitesides, L. Van de Wate, and M. Toner, Nat. Biotechnol. **20**, 826 (2002).
[5] S. Takayama, E. Ostuni, P. LeDuc, K. Naruse, D. E. Ingber, and G. M. Whitesides, Nature (London) **411**, 1016 (2001).
[6] H. B. Mao, P. S. Cremer, and M. D. Manson, Proc. Natl. Acad. Sci. U.S.A. **100**, 5449 (2003).
[7] H. P. Chou, C. Spencer, A. Scherer, and S. Quake, Proc. Natl. Acad. Sci. U.S.A. **96**, 11 (1999).
[8] L. D. Landau and E. M. Lifshitz, *Fluid Mechanics* (Pergamon, New York, 1987).
[9] L. Reyes, J. Bert, J. Fornazero, R. Cohen, and L. Heinrich, Colloids Surf., B **25**, 99 (2002).
[10] M. H. Oddy, J. G. Santiago, and J. C. Mikkelsen, Anal. Chem. **73**, 5822 (2001).
[11] J. H. Tsai and L. W. Lin, Sens. Actuators, A **97**, 665 (2002).
[12] D. Therriault, S. R. White, and J. A. Lewis, Nat. Mater. **2**, 265 (2003).
[13] R. A. Vijayendran, K. M. Motsegood, D. J. Beebe, and D. E. Leckband, Langmuir **19**, 1824 (2003).
[14] A. D. Stroock, S. K. Dertinger, A. Ajdari, I. Mezic, H. A. Stone, and G. M. Whitesides, Science **295**, 647 (2002).
[15] R. B. Bird, Ch. Curtiss, R. C. Armstrong, and O. Hassager, *Dynamics of Polymeric Liquids* (Wiley, New York, 1987).
[16] V. Tirtaatmadja and T. Sridhar, J. Rheol. **37**, 1081 (1993).
[17] D. V. Boger and K. Walter, *Rheological Phenomena in Focus* (Elsevier, Amsterdam, 1993).
[18] R. G. Larson, E. S. G. Shaqfeh, and S. J. Muller, J. Fluid Mech. **218**, 573 (1990).
[19] A. Groisman and V. Steinberg, Nature (London) **405**, 53 (2000).
[20] A. Groisman and V. Steinberg, Phys. Rev. Lett. **86**, 934 (2001).
[21] A. Groisman and V. Steinberg, Nature (London) **410**, 905 (2001).
[22] A. Groisman, M. Enzelberger, and S. R. Quake, Science **300**, 955 (2003).
[23] P. G. DeGennes, J. Chem. Phys. **60**, 5030 (1974).
[24] T. T. Perkins, D. E. Smith, and S. Chu, Science **276**, 2016 (1997).
[25] W.-M. Kulicke, M. Kotter, and H. Grager, in *Advances in Polymer Science 89,Polymer Characterization/Polymer Solutions* (Springer-Verlag, Berlin, 1989).
[26] P. J. Shrewbury, S. J. Muller, and D. Liepmann, Biomed. Microdevices **3**, 225 (2001).
[27] D. E. Smith, T. Perkins, and S. Chu, Macromolecules **29**, 1372 (1996).
[28] C. Wu, Macromolecules **26**, 3821 (1993).
[29] A. Groisman and V. Steinberg, Europhys. Lett. **43**, 165 (1998).
[30] T. Burghelea, E. Segre, and V. Steinberg, Phys. Rev. Lett. **92**, 164501 (2004).
[31] G. K. Batchelor, J. Fluid Mech. **5**, 113 (1959).
[32] M. Chertkov, G. Falkovich, I. Kolokolov, and V. Lebedev, Phys. Rev. E **51**, 5609 1995).
[33] D. T. Son, Phys. Rev. E **59**, R3811 (1999).
[34] E. Balkovsky and A. Fouxon, Phys. Rev. E **60**, 4164 (1999).
[35] D. E. Smith, H. P. Babcock, and S. Chu, Science **283**, 1724 (1999).
[36] M. A. Unger, H. P. Chou, T. Thorsen, A. Scherer, and S. R. Quake, Science **288**, 113 (2000).
[37] H. P. Chou, M. A. Unger, and S. R. Quake, Biomed. Microdevices **3**, 323 (2001).